Effect of post-heat-treatment on the structural, spectroscopic and dissolution properties of a highly stable Er3+-doped multi-component phosphate glass

Effect of post-heat-treatment on the structural, spectroscopic and dissolution properties of a highly stable Er^{3+}-doped multi-component phosphate glass

Diego Pugliese[a,*], Alexander Veber[b], Arnaud Lemière[b], Nadia G. Boetti[c], Laeticia Petit[b]

[a]Applied Science and Technology Department and INSTM Research Unit, Politecnico di Torino, Corso Duca degli Abruzzi 24, 10129 Torino, Italy

[b]Photonics Laboratory, Tampere University, PO Box 692, FI-33101 Tampere, Finland

[c]Fondazione LINKS – Leading Innovation & Knowledge for Society, Torino, Via P. C. Boggio 61, 10138 Torino, Italy

*Corresponding author. Tel: +39 0110904668, Fax: +39 0110904624. Email: diego.pugliese@polito.it

Abstract

In this paper, the impact of the post-heat-treatment on the structural and spectroscopic properties as well as on the chemical durability of a thermally stable Er^{3+}-doped phosphate glass in the system P_2O_5 - K_2O - Al_2O_3 - B_2O_3 - BaO - PbO - La_2O_3 - Gd_2O_3 is reported. Two crystalline phases, namely La, Gd-monazite and $AlKP_2O_7$, were found to precipitate from the surface of the glass after heat-treatment, as confirmed by both X-ray Diffraction (XRD) and Scanning Electron Microscopy/Energy Dispersive X-ray (SEM/EDX) analyses. Moreover, the heat-treatment was responsible for the formation of a more polymerized glass network close to the surface crystalline layer as evidenced using micro-Raman spectroscopy. From the changes in the Er^{3+} optical properties, some of the Er^{3+} ions are suspected to enter in the crystals. Both the as-prepared and heat-treated glasses were subjected to a degradation test in hydrochloric acid (HCl) and showed a congruent and incongruent dissolution behavior, respectively.

Keywords: Phosphate glass; Heat-treatment; Nucleation and growth; Glass-ceramic; Er^{3+} luminescence property; Dissolution test.

1. Introduction

In last decades, glasses and glass-ceramics (GCs) doped with rare-earth (RE) ions have been playing a key role in the development of telecommunication systems, such as optical amplifiers, solid state lasers, up-converters and 3D displays [1,2].

Among the different RE elements, Erbium is one of the most commonly used when engineering optical fiber lasers and amplifiers. Er^{3+} ions are optically pumped at around 980 or 1480 nm and then radiate light at 1530 nm with high quantum yield [3]. The 1530 nm wavelength corresponds to the intra-4f transition of Er^{3+} ions from $^4I_{13/2}$ to $^4I_{15/2}$ and is particularly important for optical communications as standard single-mode optical fibers display minimal loss at this particular wavelength [4].

Oxide glasses have proven to be stable hosts for obtaining efficient luminescence from RE ions [5]. Due to their noticeable ultra-low propagation loss and intrinsic thermo-mechanical properties, RE-doped silica-based glasses have been the material of choice for most optical fiber-related applications, showing outstanding performance in the near-infrared wavelength region [6]. However, a major bottleneck of silica glass is the poor solubility of RE ions, and the consequent tendency to cluster. This causes deleterious effects on the spectroscopic properties of the material [7]. Within this framework, intense research effort has been recently devoted to the study of novel glass families, the so-called soft glasses, which are based on alternative glass formers exhibiting different nature and structure than SiO_2. Among them, multi-component phosphate glasses have demonstrated in last years to be a true contender to silica glass as a fiber material, especially for the realization of compact active devices [8]. Their peculiar structure [9] allows them to withstand very high doping level of RE ions (up to 10^{21} ions/cm^3), which is typically about 50 times higher than in silica glass [10]. Moreover, phosphate glasses are featured by good chemical stability, easy processing, and excellent optical characteristics [1].

In recent years, the ever-increasing need to improve the optical and luminescent properties of the RE-doped glasses and consequently to boost the overall photonic devices performance has led to the development of new materials, namely the glass-ceramics. The latters combine the easy and cheap

processing technology typical of glasses with some advantages of RE-doped single crystals, such as high absorption/emission cross-section and long lifetime of luminescent levels [11]. Different routes have been adopted to fabricate GCs, the most common one consisting of a post-heat-treatment of the glass at a suitable temperature above the glass transition temperature to promote the *in situ* crystal formation in the glass matrix [2,12]. To be promising materials for photonic applications, the crystals should be homogeneously distributed in the volume of the glass matrix. Moreover, they should precipitate around the RE ions and have a specific phase to exhibit larger absorption and emission cross-sections and energy transfer rates compared to the parent glass [13]. Additionally, the GCs should be transparent and thus it is crucial to tailor both the crystal size and the refractive index difference between the crystals and the glass. Interesting results on this subject were obtained by Yu *et al.* [14], who reported an increase of about two orders of magnitude in the emission intensity at 1540 nm of the Er^{3+}/Yb^{3+} co-doped phosphate GCs compared to their glassy counterparts due to the formation of $ErPO_4$ and $YbPO_4$ nanocrystals during the heat-treatment. Recently, novel GCs in the $NaPO_3$-CaF_2 system were obtained and showed enhanced up-conversion properties compared to their parent glasses due to the volume precipitation of Er^{3+}-doped CaF_2 crystals during the heat-treatment [15,16].

The present paper reports on the study of the heat-treatment process of an Er^{3+}-doped multi-component phosphate glass featured by high thermal stability and large RE ions solubility without clustering, thus suitable for the development of compact and efficient fiber lasers and amplifiers. The glass was heat-treated using different temperatures and time intervals. The investigation of the impact of the post-heat-treatment on the morphological, structural, luminescent and dissolution properties of the glass is the major aim of the study.

2. Materials and methods

2.1 Preparation of the glass

The multi-component phosphate glass used in this work, with composition 58.76 P_2O_5 – 13.56 K_2O – 2.71 Al_2O_3 – 3.62 B_2O_3 – 4.52 BaO – 6.33 PbO – 5.25 La_2O_3 – 4.25 Gd_2O_3 – 1.00 Er_2O_3 (in mol%), was prepared by conventional melt-quenching method using chemicals with high purity level (99+%). The Er^{3+} ions

doping concentration was selected on the basis of a previous study [17] as it represents a good trade-off between a high doping level required for the fabrication of compact photonic devices and a high lifetime of the Er^{3+}:$^4I_{13/2}$ emitting level for their efficient operation. The chemicals were weighed and mixed within a dry box in order to minimize the hydroxyl ions (OH^-) content in the glass. The batched chemicals were melted in an alumina crucible in a vertical furnace at a temperature of 1400 °C for 1 h under controlled atmosphere. The melt was cast into a preheated cylindrical brass mold 12 mm in diameter, then annealed at a temperature around the transition temperature, T_g, for 5 h to relieve glass internal stresses, and finally cooled down slowly to room temperature. After annealing, the as-prepared glass was cut into 5 mm-thick disks and post-heat-treated with a heating ramp of 20 °C/min at (T_g + 20 °C) for 17 h to start nucleation and then at higher temperatures from 6 to 96 h to grow the nuclei into the crystals. For the heat-treatment, the glass disks were placed on a platinum foil to prevent any contamination from the sample holder. The heat-treatments were performed in air.

For the dissolution experiments, the glasses prior to and after the heat-treatment at (T_g + 20 °C) for 17 h and at the crystallization peak temperature (T_p) for 16 h were soaked in a 37 wt% HCl solution at room temperature for 5 days. The geometry of the samples was approximately 5 mm x 6 mm x 1.2 mm and the acid volume/glass mass ratio was 0.13 ml/mg. The acid was changed every day to avoid solution saturation effects. The samples were periodically weighed over the whole dissolution time, thus making possible to estimate their etching rate.

2.2 Characterization

The density (ρ) of the glass was measured at room temperature by the Archimedes' method using distilled water as immersion fluid. The accuracy of the measurement is ± 0.05 g/cm^3. The Er^{3+} ions concentration was calculated from the measured sample density and its initial composition.

The T_g and T_p of the as-prepared glass were measured through differential thermal analysis (DTA) (Netzsch JUPITER F1 instrument) at the heating rate of 10 °C/min in Pt crucible. The T_g was determined as the inflection point of the endotherm obtained by taking the minimum of first derivative of the DTA curve,

while T_p was taken as the maximum peak of the exotherm. The onset of the crystallization peak, T_x, was also measured. All measurements were performed with an accuracy of ± 3 °C.

The glass coefficient of thermal expansion (CTE) was measured with a horizontal alumina dilatometer (Netzsch, DIL 402 PC) on a 5 mm-long specimen operating at 5 °C/min up to 1200 °C. The measure was automatically interrupted when shrinkage higher than 0.13% was reached (softening point, T_s). The CTE value was calculated in the 200-400 °C temperature range, featuring an error of ± 0.1 $°C^{-1}$.

An X-ray Diffraction (XRD) analyzer (PANalytical Empyrean) with Co K_α X-ray radiation (λ = 1.79 Å) was used to identify the crystalline phases in the heat-treated glasses. Data were collected from 2θ = 20 up to 60° with a step size of 0.013°.

The composition and morphology of the glass prior to and after the heat-treatment were investigated using a Scanning Electron Microscope (Crossbeam 540 Carl Zeiss) equipped with an Energy Dispersive Spectroscopy (EDS/EDX) detector (Oxford Instruments X-MaxN 80). The samples were mounted on Al-stubs and coated with a thin carbon layer prior to the SEM/EDX analysis. The detection limit of the EDX system was ± 0.5 at.%.

The Raman spectra of the glass prior to and after the heat-treatment were acquired with a Renishaw inVia Qontor Raman microscope equipped with a cooled charge coupled device (CCD) camera using a 405 nm laser for the excitation. A linear Raman mapping was also performed on the cross-section of the heat-treated glass sample; the mapping line was perpendicular to the edge of the sample and spanned the surface crystalline layer and the internal glassy part.

The emission spectra of the glass and GCs were measured in the 1400-1700 nm range at room temperature using a continuous-wave (CW) 970 nm laser diode for excitation. The spectra were acquired using a Spectro 320-131 optical spectrum analyzer (Instrument Systems Optische Messtechnik GmbH, Germany) equipped with an InGaAs detector for wavelengths ranging from 800 to 1700 nm.

The fluorescence lifetime of the Er^{3+}:$^4I_{13/2}$ level was obtained by exciting the glass and GC samples with a fiber pigtailed laser diode operating at the wavelength of 976 nm in pulsed mode, acquiring emission by means of an InGaAs amplified detector (Thorlabs PDA10CS2), recording the signal by an universal serial bus (USB)-oscilloscope (Picoscope 5242D) and fitting the decay traces by single exponential function. The

measurement was performed by exciting the bulk samples at their very edge to minimize reabsorption. Estimated error of the measurement was ± 0.2 ms.

3. Results and discussion

The as-prepared multi-component phosphate glass showed a good homogeneity and the absence of crystals, as assessed through a visual inspection. The exothermic crystallization peak was detected only for the fine-powdered glass sample (see Fig. 1), thus clearly indicating that the synthesized glass is rather stable against crystallization. The physical and thermo-mechanical properties of the as-prepared glass are summarized in Table 1.

Table 1

Density (ρ), glass transition temperature (T_g), onset crystallization temperature (T_x), crystallization peak temperature (T_p), glass thermal stability ($\Delta T = T_x - T_g$), coefficient of thermal expansion (CTE), softening temperature (T_s) and Er^{3+} ions concentration of the as-prepared phosphate glass. T_x and T_p temperatures were determined from the fine-powdered glass DTA curve.

ρ [g/cm^3] ± 0.05 g/cm^3	T_g [°C] ± 3 °C	T_x [°C] ± 3 °C	T_p [°C] ± 3 °C	$\Delta T = T_x - T_g$ [°C] ± 6 °C	CTE [× 10^{-6} °C^{-1}] ± 0.1 °C^{-1}	T_s [°C] ± 3 °C	Er^{3+} [× 10^{20} ions/cm^3] ± 0.04 ions/cm^3
3.41	510	705	750	195	9.0	529	2.59

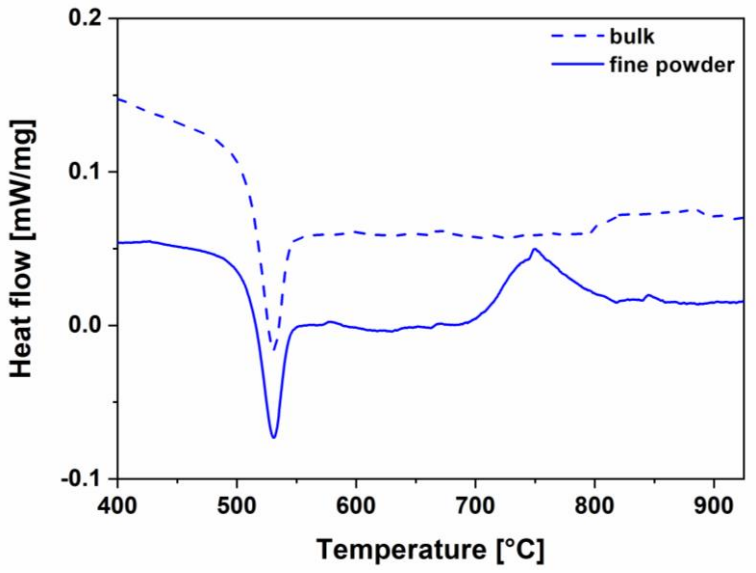

Fig. 1. DTA thermograms of the as-prepared bulk and fine-powdered phosphate glass. Fine powder was used to evidence the crystallization peak.

The glass exhibited higher T_g and lower CTE values than those reported in literature for other phosphate glass compositions [18,19], proving that it is markedly robust and resistant to the thermal stress induced by its processing. Moreover, a glass stability parameter ΔT of ~200 °C was assessed, thus indicating that the synthesized glass is stable against devitrification and suitable for crystal-free fiber drawing. The enhanced thermal stability and solubility toward Er^{3+} ions exhibited by the investigated phosphate glass make it a promising platform for the development of compact and efficient eye-safe fiber laser sources operating at 1550 nm.

The glass was heat-treated at (T_g + 20 °C) for 17 h and then at higher temperatures ranging from 650 to 750 °C for 16 to 96 h. After the heat-treatment, the glasses were opaque and they also lost their shape due to an excessive viscous flow. The XRD patterns of some heat-treated glasses are reported in Fig. 2.

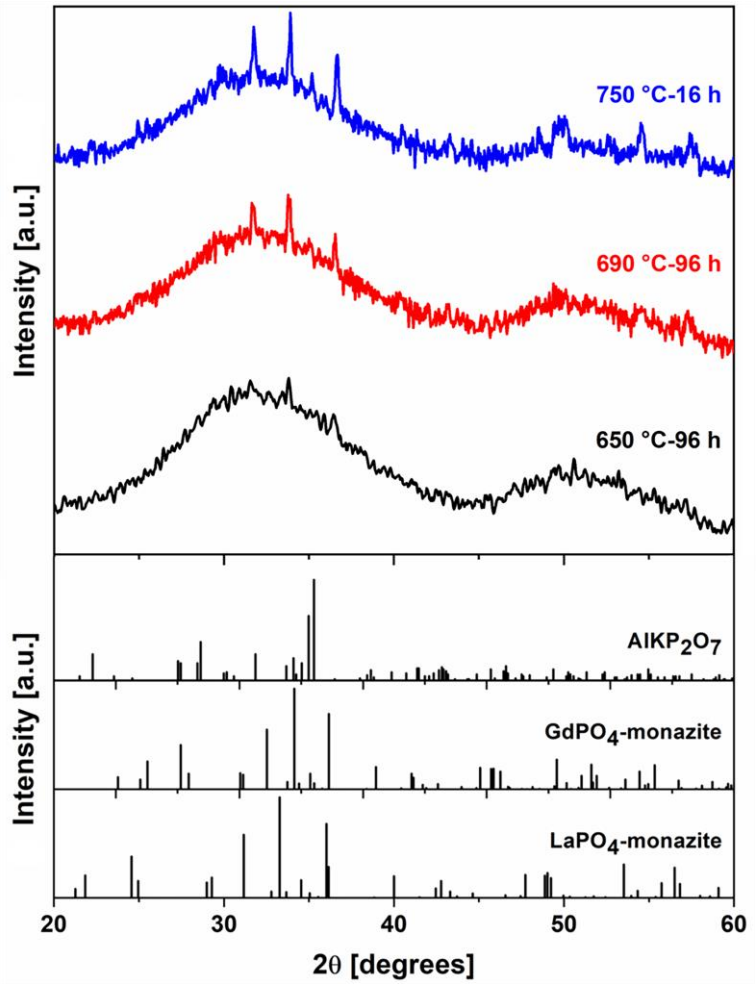

Fig. 2. XRD patterns of the glass heat-treated at (T_g + 20 °C) for 17 h and then at 650, 690 and 750 °C for different time intervals. The XRD patterns of the suspected crystals are also shown.

Two crystalline phases, i.e. RE-monazite and $AlKP_2O_7$, were found to precipitate in the glass. One should point out that the peaks' position of the RE-monazite phase does not perfectly match neither the XRD pattern of $LaPO_4$-monazite nor that of $GdPO_4$-monazite. RE-monazites exhibit similar XRD patterns in experiment, the position of the diffraction peaks depending on the RE ions. Based on the literature data, $La_{1-x}Gd_xPO_4$-monazite solid solution is suspected to precipitate during the heat-treatment [20,21].

The morphology and the composition of the cross-section of the glass heat-treated at (T_g + 20 °C) for 17 h and at 750 °C for 16 h were analyzed using SEM/EDX. The SEM image of the cross-section of the heat-treated glass, depicted in Fig. 3a, clearly shows that the crystal formation mechanism is a surface crystallization, i.e. no crystals could be found in the volume of the glass. The composition at the central part

of the heat-treated glass was found to be similar to that of the as-prepared glass, while abrupt compositional changes were detected near the surface (see Fig. 3b).

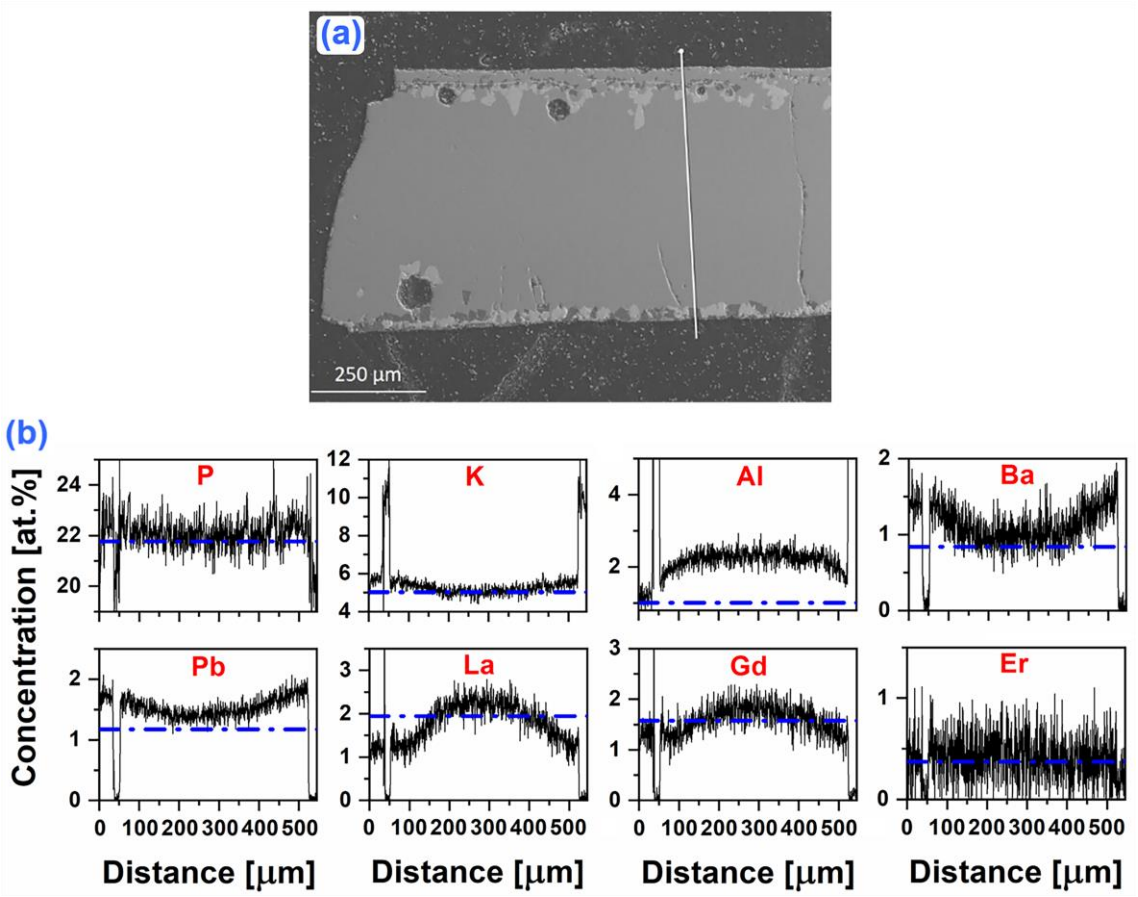

Fig. 3. SEM image (a) and EDX concentration profile (b) of the cross-section of the glass heat-treated at (T_g + 20 °C) for 17 h and then at 750 °C for 16 h. The white line in (a) shows the EDX mapping trajectory, the concentration profiles in (b) are given only when measured in the sample (embedding epoxy region is excluded). The dashed-dot blue lines in (b) represent the expected at.% of all the elements.

An individual EDX mapping of the surface layer of the heat-treated glass was also acquired (see Fig. 4).

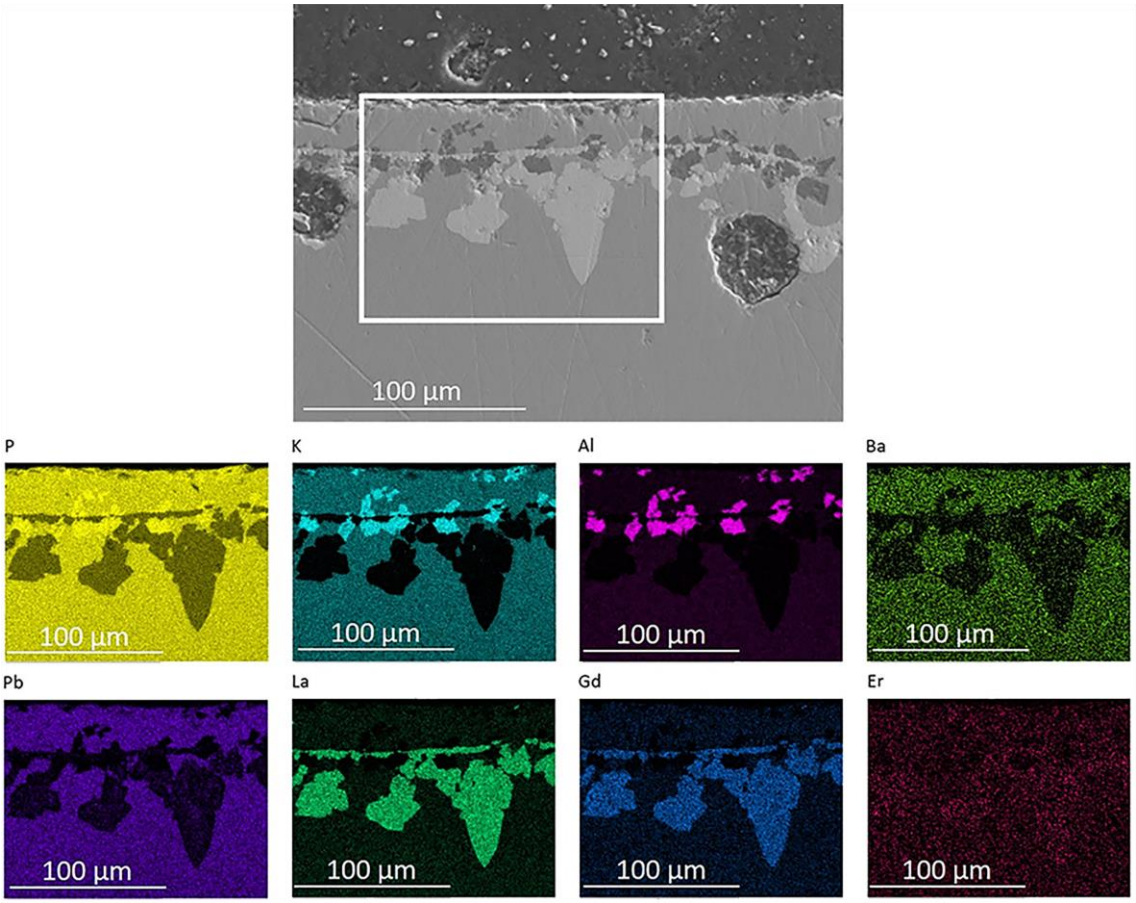

Fig. 4. EDX mapping of the surface layer of the glass heat-treated at (T_g + 20 °C) for 17 h and then at 750 °C for 16 h. The white rectangle in the top panel highlights the mapped sample region, brighter areas indicate higher element content.

Areas with K-, Al-, La- and Gd-rich compositions are visible at different spots, thus confirming the precipitation of the RE-monazite and $AlKP_2O_7$ crystalline phases at the surface of the glass after the post-heat-treatment.

The micro-Raman spectra of the glass heat-treated at (T_g + 20 °C) for 17 h and then at 750 °C for 16 h measured close to and far from the surface crystalline layer are presented in Fig. 5a. The spectra were normalized to the band peaking at ~1165 cm^{-1}. The spectra exhibit bands at ~700, 800-1050, ~1165 and 1200-1300 cm^{-1}. According to what reported by Konidakis *et al.* [22], the band at ~700 cm^{-1} is assigned to the symmetric stretching of P-O-P bridges. The bands at ~930, 1030 and 1100 cm^{-1} can be related to the symmetric PO_4 stretching on Q^0 tetrahedra and to the symmetric and asymmetric PO_3 stretching on Q^1 tetrahedra, respectively [23]. The bands at around 1165 and 1250 cm^{-1} can be ascribed to the symmetric and

asymmetric stretching of Q^2 groups, respectively [24]. Finally, the shoulder at 1300 cm^{-1} reveals the presence of Q^3 groups in small amount.

The spectrum acquired close to the crystalline layer exhibits a slightly lower intensity of the bands related to $\nu_s(Q^0)$, $\nu_s(Q^1)$ and $\nu_{as}(Q^1)$ compared to the spectrum acquired far from the crystalline layer. This is a clear indication of chemical elements redistribution occurring during the heat-treatment, which leads to the decrease in the number of non-bridging oxygens (NBOs) and consequently to the increase in the degree of polymerization of the phosphate glass network close to the crystalline layer. A linear Raman mapping was measured across the heat-treated glass to further evidence the changes in the glass structure due to the redistribution of the elements. The mapping line was perpendicular to the edge of the sample and spanned both the surface crystalline layer and the internal glassy parts of the sample. Fig. 5b shows the ratio between Raman signal intensities at ~1165 and ~1030 cm^{-1}. This ratio approaches the value obtained for the as-prepared glass at about 120 μm, which agrees well with the EDX data shown in Fig. 3b and confirms once again that no or very minor structural changes occurred in the volume of the glass during the heat-treatment.

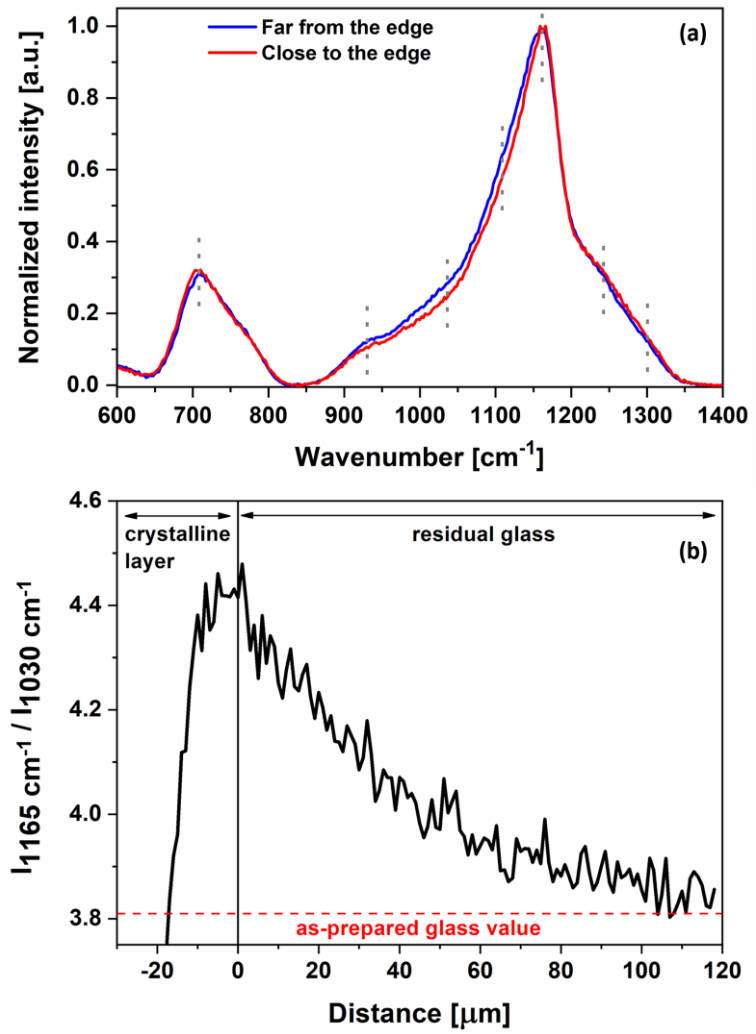

Fig. 5. (a) Normalized Raman spectra of the glass heat-treated at (T_g + 20 °C) for 17 h and then at 750 °C for 16 h collected close to and far from the surface crystalline layer. The main bands were marked by dotted gray lines as a guide to the eyes. (b) Ratio between Raman signal intensities at ~1165 and 1030 cm^{-1} across the glass heat-treated at 750 °C for 16 h obtained from the linear Raman mapping. The horizontal dashed red line corresponds to the value for the as-prepared glass.

The spectroscopic properties of the glass were measured prior to and after the heat-treatment. Interestingly, the heat-treatment of the glass showed a minor effect on the shape of the Er^{3+} ions emission band centered at around 1550 nm (see Fig. 6a). These minor differences can be detected only after the heat-treatment at higher temperatures and for a longer time, in particular some low intensity narrow bands can be distinguished at ~1500 and 1520 nm after the treatment at 750 °C for 16 h. At the same time, the heat-treatment led to a noticeable decrease in the integral emission intensity (see Fig. 6b) and also to the reduction of the Er^{3+}:$^4I_{13/2}$ excited state lifetime (see Fig. 6c and Table 2).

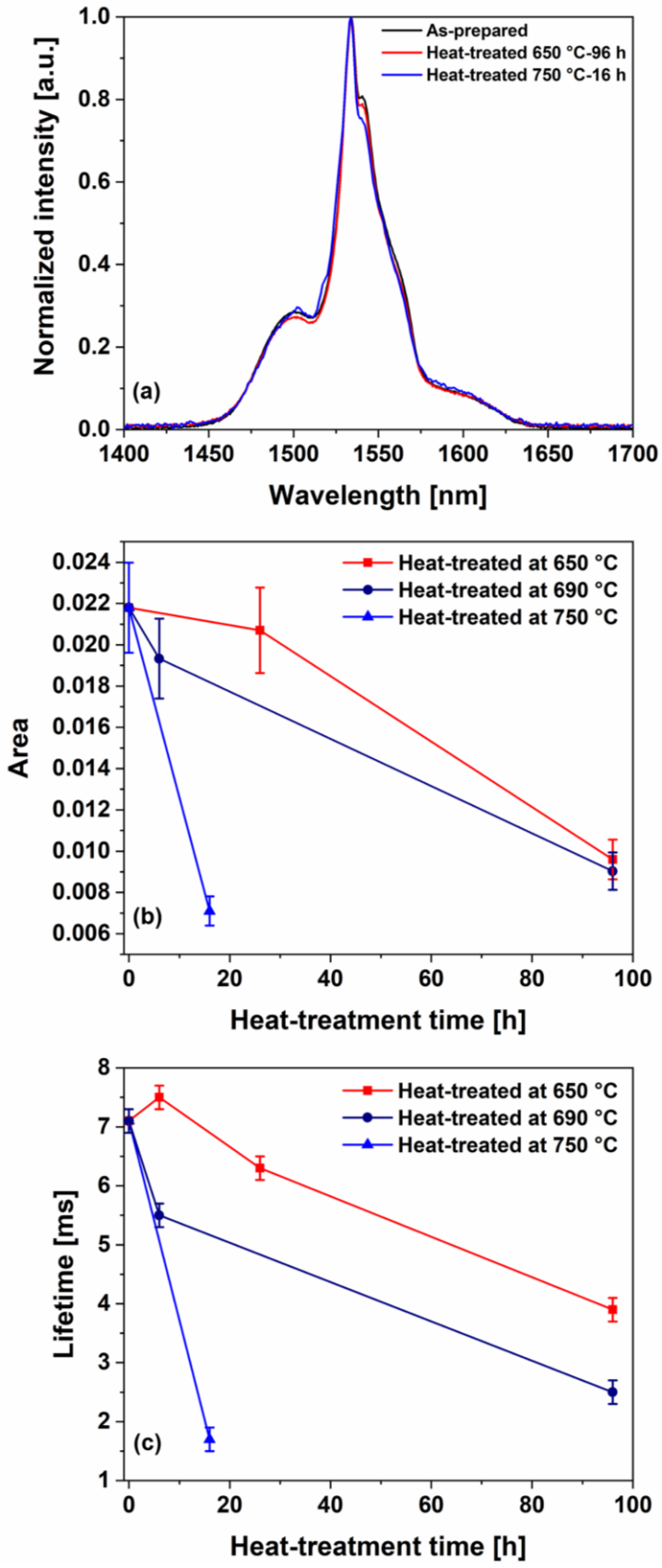

Fig. 6. (a) Normalized emission spectra measured at the surface of the glass prior to and after the heat-treatment. (b) Area of the Er^{3+} ions emission band centered at around 1550 nm measured from the glass prior to and after the heat-

treatment crushed into powder. (c) Er^{3+}:$^4I_{13/2}$ excited state lifetime values of the glass prior to and after the heat-treatment.

Table 2

Excited state Er^{3+}:$^4I_{13/2}$ lifetime values of both untreated and post-heat-treated Er^{3+}-doped phosphate glasses measured under laser excitation at 976 nm.

Thermal treatment	**Er^{3+}:$^4I_{13/2}$ lifetime [ms] ± 0.2 ms**
Untreated glass	7.1
650 °C-6 h	7.5
650 °C-26 h	6.3
650 °C-96 h	3.9
690 °C-6 h	5.5
690 °C-96 h	2.5
750 °C-16 h	1.7

Due to the similarity in ionic radii of Er^{3+}, Gd^{3+} and La^{3+} ions, it is reasonable to assume that the changes in the Er^{3+} ions spectroscopic properties are due to the incorporation of some of the Er^{3+} ions in the monazite crystalline phase. Indeed, an Er^{3+}:$^4I_{13/2}$ excited state lifetime value of ~3.7 ms and a quantum efficiency, defined as the ratio of the measured luminescence lifetime to the radiative lifetime, of about 50% were reported for Er^{3+}-doped La-monazite [25]. As the quantum efficiency can be above 70% in the case of phosphate glasses [26], the intensity of the emission at 1550 nm of the investigated glass is expected to decrease after the heat-treatment due to the precipitation of Er^{3+}-doped monazite phase. Moreover, in the most crystallized sample (750 °C-16 h) the presence of short and long lifetime components in the luminescence decay law was clearly detected, and the long component slope was found close to the one of the as-prepared glass decay curve (see Fig. 7). This supports our assumption about the presence of Er^{3+} ions in two different phases after devitrification.

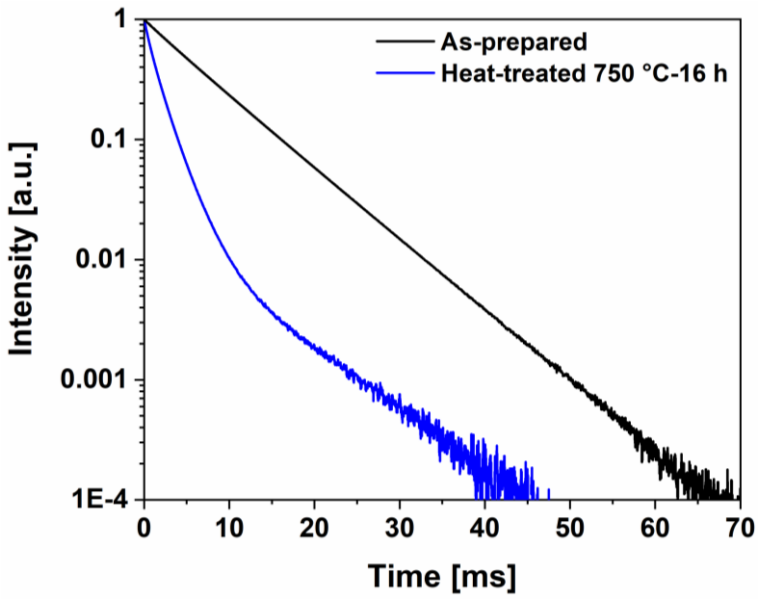

Fig. 7. Emission decay curves of the as-prepared glass and 750 °C-16 h GC samples.

It is well known that the RE-phosphate crystals are chemically and thermally durable materials [27–29]. Therefore to confirm the incorporation of Er^{3+} ions in the monazite phase, a leaching experiment of the glass prior to and after heat-treatment at (T_g + 20 °C) for 17 h and then at 750 °C for 16 h was performed. The glasses prior to and after the heat-treatment were immersed in a 37 wt% HCl solution at room temperature for 5 days, and the samples were weighed over the whole dissolution time. The mass values of the glasses after 24, 48 and 120 h of soaking in HCl are reported in Fig. 8. The linear fitting of the experimental data allowed assessing the etching rate values for both the untreated and thermally treated glasses, which revealed to be equal to (1.04 ± 0.11) and (0.84 ± 0.11) mg/day, respectively, i.e. dissolution rates of the glass and the GC are the same within the experimental error.

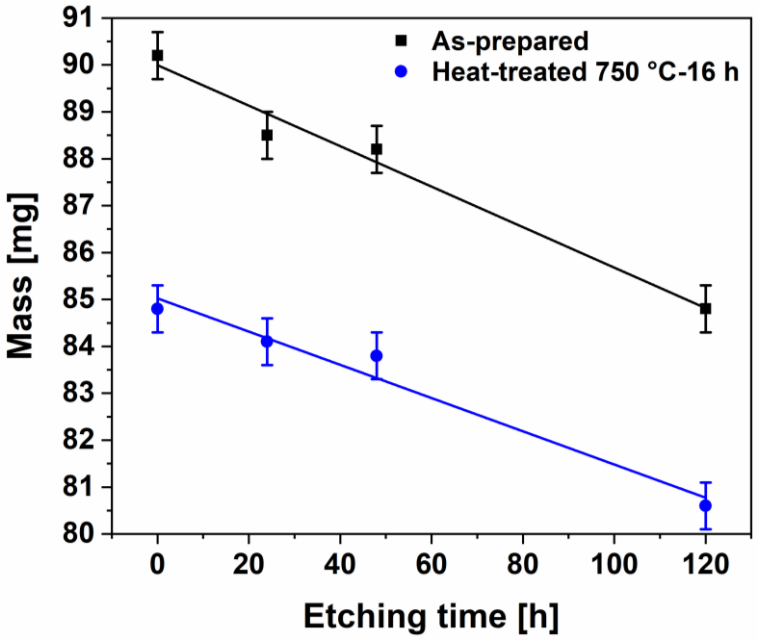

Fig. 8. Mass values of the glass prior to and after the heat-treatment at (T_g + 20 °C) for 17 h and then at 750 °C for 16 h as a function of the etching time. The points are experimental data, while the continuous lines are linear fitting curves.

The normalized emission spectra in the 1400-1700 nm range of the as-prepared glass and of the glass heat-treated at (T_g + 20 °C) for 17 h and then at 750 °C for 16 h prior to and after etching in HCl for 120 h are reported in Fig. 9.

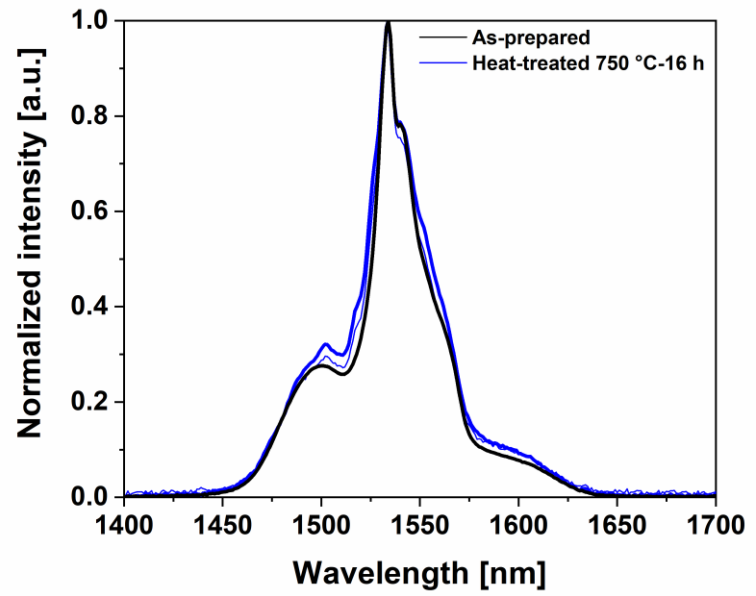

Fig. 9. Normalized emission spectra of the as-prepared glass and of the glass after the heat-treatment at (T_g + 20 °C) for 17 h and then at 750 °C for 16 h prior to (thin line) and after (thick line) etching in HCl for 120 h. The spectra were measured from the surface of the glass.

No changes in the shape nor in the intensity of the Er^{3+} ions emission band centered at around 1550 nm were observed after immersing the as-prepared glass for 120 h in HCl. The composition of the as-prepared glass was also found to be unchanged after the etching process, i.e. the glass itself dissolved congruently in HCl. However, small changes in the shape of the emission could be highlighted after immersing the heat-treated glass in HCl for 120 h: the narrow bands at ~1500 and 1520 nm became more prominent and the intensity of the shoulders at ~1500 and 1550 nm increased as compared to the main band. One should also mention that the intensity of the emission was found to remain unchanged after immersing the heat-treated glass for 120 h in HCl. Taking into account the high chemical durability of RE-monazite, the glass should be less stable against HCl treatment than the heat-treated glass. While the composition of the as-prepared glass was found to be unchanged after the etching process, the composition of the heat-treated glass changed after being immersed in HCl: both Al-rich and La-Gd-rich compositions were detected on different spots at the surface of the sample after the etching experiment indicating that the glass is less chemically stable than RE-phosphate crystals in HCl. Thus the leaching increased the crystallinity of the glass surface making more obvious the fact that some Er^{3+} ions were incorporated in the precipitated crystalline phases.

4. Conclusions

In conclusion, an Er^{3+}-doped phosphate glass in the system P_2O_5 - K_2O - Al_2O_3 - B_2O_3 - BaO - PbO - La_2O_3 - Gd_2O_3 was successfully synthesized by melt-quenching technique. The glass displays a good thermal stability and it is able to host a considerably high-volume concentration of Er^{3+} ions, i.e. ~2.6×10^{20} ions/cm^3, hence it can be regarded as a promising candidate to be drawn into an active optical fiber for compact and efficient eye-safe laser sources. The glass was heat-treated at different temperatures in the 650-750 °C range and for different time intervals varying from 6 to 96 h to induce the precipitation of crystals. The heat-treatment led to surface crystallization. Based on the XRD and SEM/EDX analyses, La, Gd-monazite and $AlKP_2O_7$ are the main crystalline phases precipitating at the surface of glass. Using micro-Raman spectroscopy, it was shown that the crystallization led to the redistribution of the chemical elements in the sample and to the formation of more polymerized glass close to the surface crystalline layer. The observed changes in the spectroscopic properties induced by the heat-treatment indicate that some of the Er^{3+} ions remained in the amorphous part of the heat-treated glass while others were incorporated in the RE-monazite formed upon crystallization. The latter was additionally confirmed by leaching of the samples in HCl. The glass prior to and after the heat-treatment showed a congruent and incongruent dissolution behavior, respectively, due to the higher chemical durability of the RE-monazite and $AlKP_2O_7$ crystals than the glass in HCl. HCl.

CRediT authorship contribution statement

Diego Pugliese: Conceptualization, Methodology, Validation, Investigation, Writing - original draft, Visualization. **Alexander Veber:** Validation, Investigation, Writing - review & editing. **Arnaud Lemière:** Validation, Investigation, Writing - review & editing. **Nadia G. Boetti:** Investigation, Writing - review & editing. **Laeticia Petit:** Conceptualization, Methodology, Resources, Writing - review & editing, Visualization, Supervision.

Declaration of competing interest

The authors declare that they have no known competing financial interests or personal relationships that could have appeared to influence the work reported in this paper.

Acknowledgements

D.P. acknowledges the Interdepartmental Center "PhotoNext" of Politecnico di Torino for the partial support of this research effort. Academy of Finland (Flagship Programme, Photonics Research and Innovation PREIN-320165 and Academy Project - 326418) is greatly acknowledged for the financial support. This work made use of Tampere Microscopy Center facilities at Tampere University.

References

1. M. Yamane, Y. Asahara, Glasses for Photonics, first ed., Cambridge University Press, Cambridge, 2000.

2. M.J. Dejneka, Transparent oxyfluoride glass ceramics, MRS Bull. 23 (1998) 57–62.

3. M. Dubinskii, J. Zhang, V. Ter-Mikirtychev, Highly scalable, resonantly cladding-pumped, Er-doped fiber laser with record efficiency, Opt. Lett. 34 (2009) 1507–1509.

4. W.J. Miniscalco, Erbium-doped glasses for fiber amplifiers at 1500 nm, J. Lightwave Technol. 9 (1991) 234–250.

5. A. Martucci, A. Chiasera, M. Montagna, M. Ferrari, Erbium-doped GeO_2–TiO_2 sol–gel waveguides, J. Non-Cryst. Solids 322 (2003) 295–299.

6. M.J.F. Digonnet, Rare-Earth-Doped Fiber Lasers and Amplifiers, second ed., CRC Press, Boca Raton, 2001.

7. R.S. Quimby, W.J. Miniscalco, B. Thompson, Clustering in erbium-doped silica glass fibers analyzed using 980 nm excited-state absorption, J. Appl. Phys. 76 (1994) 4472–4478.

8. T. Qiu, L. Li, A. Schülzgen, V.L. Temyanko, T. Luo, S. Jiang, A. Mafi, J.V. Moloney, N. Peyghambarian, Generation of 9.3-W multimode and 4-W single-mode output from 7-cm short fiber lasers, IEEE Photonics Technol. Lett. 16 (2004) 2592–2594.

9. K. Seneschal, F. Smektala, B. Bureau, M. Le Floch, S. Jiang, T. Luo, J. Lucas, N. Peyghambarian, Properties and structure of high erbium doped phosphate glass for short optical fibers amplifiers, Mater. Res. Bull. 40 (2005) 1433–1442.

10. N.G. Boetti, D. Pugliese, E. Ceci-Ginistrelli, J. Lousteau, D. Janner, D. Milanese, 2017. Highly doped phosphate glass fibers for compact lasers and amplifiers: a review. Appl. Sci. 7, 1295.

11. G. Dantelle, M. Mortier, D. Vivien, G. Patriarche, Influence of Ce^{3+} doping on the structure and luminescence of Er^{3+}-doped transparent glass-ceramics, Opt. Mater. 28 (2006) 638–642.

12. P. Lopez-Iscoa, T. Salminen, T. Hakkarainen, L. Petit, D. Janner, N.G. Boetti, M. Lastusaari, D. Pugliese, P. Paturi, D. Milanese, 2017. Effect of partial crystallization on the structural and luminescence properties of Er^{3+}-doped phosphate glasses. Materials. 10, 473.

13. M.C. Gonçalves, L.F. Santos, R.M. Almeida, Rare-earth-doped transparent glass ceramics, CR Chim. 5 (2002) 845–854.

14. X. Yu, F. Song, W. Wang, L. Luo, L. Han, Z. Cheng, T. Sun, J. Tian, E.Y.B. Pun, 2008. Comparison of optical parameters and luminescence between Er^{3+}/Yb^{3+} codoped phosphate glass ceramics and precursor glasses. J. Appl. Phys. 104, 113105.

15. N. Ojha, A. Szczodra, N.G. Boetti, J. Massera, L. Petit, Nucleation and growth behavior of Er^{3+} doped oxyfluorophosphate glasses, RSC Adv. 10 (2020) 25703–25716.

16. A. Szczodra, A. Mardoukhi, M. Hokka, N.G. Boetti, L. Petit, Fluorine losses in Er^{3+} oxyfluoride phosphate glasses and glass-ceramics, J. Alloys Compd. 797 (2019) 797–803.

17. D. Pugliese, N.G. Boetti, J. Lousteau, E. Ceci-Ginistrelli, E. Bertone, F. Geobaldo, D. Milanese, Concentration quenching in an Er-doped phosphate glass for compact optical lasers and amplifiers, J. Alloys Compd. 657 (2016) 678–683.

18. Q. Yin, S. Kang, X. Wang, S. Li, D. He, L. Hu, Effect of PbO on the spectral and thermo-optical properties of Nd^{3+}-doped phosphate laser glass, Opt. Mater. 66 (2017) 23–28.

19. P. Lopez-Iscoa, L. Petit, J. Massera, D. Janner, N.G. Boetti, D. Pugliese, S. Fiorilli, C. Novara, F. Giorgis, D. Milanese, Effect of the addition of Al_2O_3, TiO_2 and ZnO on the thermal, structural and luminescence properties of Er^{3+}-doped phosphate glasses, J. Non-Cryst. Solids 460 (2017) 161–168.

20. O. Terra, N. Clavier, N. Dacheux, R. Podor, Preparation and characterization of lanthanum–gadolinium monazites as ceramics for radioactive waste storage, New J. Chem. 27 (2003) 957–967.

21. N. Clavier, R. Podor, N. Dacheux, Crystal chemistry of the monazite structure, J. Eur. Ceram. Soc. 31 (2011) 941–976.

22. I. Konidakis, C.-P.E. Varsamis, E.I. Kamitsos, D. Möncke, D. Ehrt, Structure and properties of mixed strontium–manganese metaphosphate glasses, J. Phys. Chem. C 114 (2010) 9125–9138.

23. R.K. Brow, Review: the structure of simple phosphate glasses, J. Non-Cryst. Solids 263–264 (2000) 1–28.

24. M.A. Karakassides, A. Saranti, I. Koutselas, Preparation and structural study of binary phosphate glasses with high calcium and/or magnesium content, J. Non-Cryst. Solids 347 (2004) 69–79.

25. R. Lisiecki, W. Ryba-Romanowski, A. Speghini, M. Bettinelli, Luminescence spectroscopy of Er^{3+}-doped and Er^{3+}, Yb^{3+}-codoped $LaPO_4$ single crystals, J. Lumin. 129 (2009) 521–525.

26. A. Amarnath Reddy, S. Surendra Babu, K. Pradeesh, C.J. Otton, G. Vijaya Prakash, Optical properties of highly Er^{3+}-doped sodium–aluminium–phosphate glasses for broadband 1.5 μm emission, J. Alloys Compd. 509 (2011) 4047–4052.

27. Y. Hikichi, T. Nomura, Melting temperatures of monazite and xenotime, J. Am. Ceram. Soc. 70 (1987) C-252–C-253.

28. Y. Hikichi, T. Ota, K. Daimon, T. Hattori, M. Mizuno, Thermal, mechanical, and chemical properties of sintered xenotime-type RPO4 (R = Y, Er, Yb, or Lu), J. Am. Ceram. Soc. 81 (1998) 2216–2218.

29. L.A. Boatner, M.M. Abraham, B.C. Sales, Lanthanide orthophosphate ceramics for the disposal of actinide-contaminated nuclear wastes, Inorg. Chim. Acta 94 (1984) 146–148.